Spectrochimica Acta Part B 64 (2009) 1259–1265

Contents lists available at ScienceDirect

Spectrochimica Acta Part B

journal homepage: www.elsevier.com/locate/sab

Isotope ratio analysis on micron-sized particles in complex matrices by Laser Ablation-Absorption Ratio Spectrometry

B.A. Bushaw [a], N.C. Anheier Jr. [b,*]

[a] Fundamental and Computational Sciences Directorate, Pacific Northwest National Laboratory, Richland, WA 99352, United States
[b] National Security Directorate, Pacific Northwest National Laboratory, Richland, WA 99352, United States

ARTICLE INFO

Article history:
Received 25 August 2009
Accepted 13 October 2009
Available online 18 October 2009

Keywords:
Laser ablation
Diode laser absorption
Isotope ratio
Particulate
Gadolinium

ABSTRACT

Laser ablation has been combined with dual tunable diode laser absorption spectrometry to measure ^{152}Gd:^{160}Gd isotope ratios in micron-size particles. The diode lasers are tuned to specific isotopes in two different atomic transitions at 405.9 nm (^{152}Gd) and 413.4 nm (^{160}Gd) and directed collinearly through the laser ablation plume, separated on a diffraction grating, and detected with photodiodes to monitor transient absorption signals on a shot-by-shot basis. The method has been characterized first using Gd metal foil and then with particles of $GdCl_3 \cdot xH_20$ as binary and ternary mixtures with ^{152}Gd:^{160}Gd isotope ratios ranging from 0.01 to 0.43. These particulate mixtures have been diluted with Columbia River sediment powder (SRM 4350B) to simulate environmental samples and we show the method is capable of detecting a few highly-enriched particles in the presence of a >100-fold excess of low-enrichment particles, even when the Gd-bearing particles are a minor component (0.08%) in the SRM powder and widely dispersed (1178 particles detected in 800,000 ablation laser shots). The implications for monitoring ^{235}U:^{238}U enrichment ratios in airborne particle samples, as related to the nuclear industry, are discussed.

1. Introduction

Laser ablation has a long and successful history as a direct sampling method for trace analysis [1,2]. Methods that interrogate the material ablated from the solid sample include passive use of the particulate matter generated, e.g., entraining in a gas flow feeding inductively-coupled-plasmas with mass-spectrometric (ICP-MS) or atomic emission (ICP-AES) detection and 'passive' observation of the ablation/plasma formation process, such as in laser induced 'breakdown' spectroscopy (LIBS) [3]. The laser ablation plume also may be actively interrogated by methods such as laser induced fluorescence [4], or absorption [5,6]. In this paper we describe the application of Laser Ablation-Absorption Ratio Spectrometry (LAARS) to measuring isotope ratios for a targeted element in individual micron-sized particles that are themselves minor components in a larger heterogeneous mix of 'background' particles. This composition is consistent with swipe and environmental aerosol samples collected by nuclear safeguard inspectors. The method uses two wavelength tunable diode lasers to simultaneously probe the absorption of the ablation plume on two different atomic transitions, with each laser tuned to a specific isotope within its respective transition. This is similar to the dual-probe-laser approach used in [6]; however, that work applied nearly identical lasers to different isotopes within the same transition and, because of the nearly identical wavelengths of the lasers, spatially separated them (crossing angle of 4°) for independent detection. In contrast, we use different wavelength lasers that are precisely collinear through the ablation plume and are then separated with a diffraction grating before detection.

This method is ultimately targeted for the measurement of ^{235}U:^{238}U in support of nuclear fuel cycle safeguards and nonproliferation efforts; however, for the development and characterization described here, we used gadolinium as a surrogate. While the chemistry and atomic spectroscopy of U and Gd are quite similar, Gd is non-radioactive and has only limited health concerns. Gd has a number of naturally occurring isotopes (152, 154, 155, 156, 157, 158, and 160), and the 152:160 pair is suitable as a uranium surrogate because the natural abundance ratio $R = 0.0091$ is similar to $R = 0.0073$ for natural ^{235}U:^{238}U, and typical optical isotope shifts in both pairs are on the order of 10 GHz. ^{235}U will have hyperfine structure (hfs); thus, selection of strong transitions [7], with hfs width [8–15] comparable to or less than the Doppler width, and large isotope shift [16,17] will be important for maximizing sensitivity, dynamic range, and isotopic selectivity.

2. Experimental

2.1. Instrumentation

Fig. 1 shows an overall schematic for the LAARS instrumentation. Solid samples are mounted on a XY-Z micropositioner within a reduced pressure (~1300 Pa argon) measurement chamber. The motorized X and Y stages (Numerical Aperture Inc. model MM-3M-F) are used to

* Corresponding author. Tel.: +001 509 375 2639.
E-mail address: norm.anheier@pnl.gov (N.C. Anheier).

0584-8547/$ – see front matter © 2009 Elsevier B.V. All rights reserved.
doi:10.1016/j.sab.2009.10.002

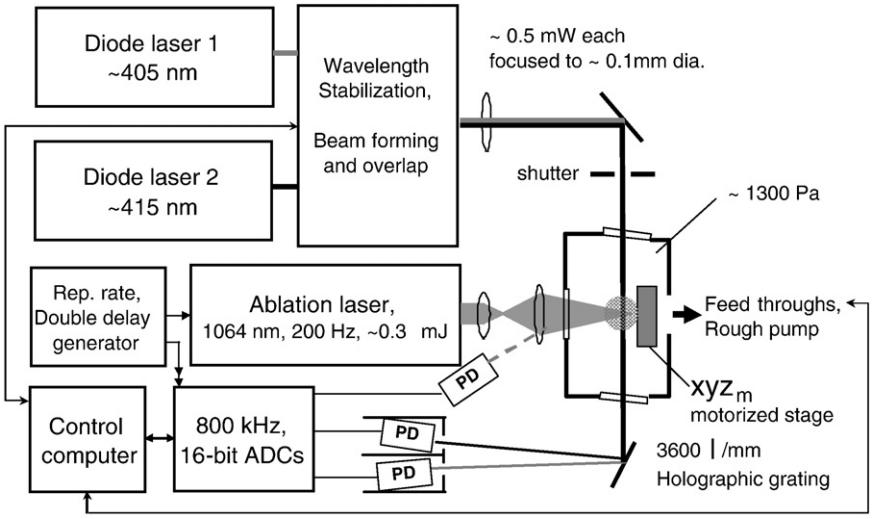

Fig. 1. Experimental apparatus for Laser Ablation-Absorption Ratio Spectrometry (LAARS) measurement of isotope ratios in particulate samples. 'PD' are amplified Si-PIN photodiodes.

raster the sample surface under the ablation laser (CryLas model DSS1064-450 diode pumped Nd:YAG: 200 Hz, ≈300 μJ, 1 ns pulses), while the Z section is manually tuned to adjust the focal depth and the height of the probe lasers above the surface. The sample is typically scanned at 4 mm/s and the laser spot diameter is ≈20 μm. The probe lasers are external cavity violet diode lasers (Toptica DL100) running near 405 and 415 nm. The outputs of these are sampled and wavelength monitored with a high-resolution wavelength meter (Burleigh WA1500), which is used to correct long-term wavelength drift. Without correction, the diode laser frequencies may drift several hundreds of MHz/h; with correction there is essentially no long-term drift, but precision of the wavemeter increases the effective laser linewidths from ~1 to ~10 MHz. However, this is inconsequential when studying Doppler broadened transitions with ~1 GHz absorption linewidth. The beams are spatially filtered through alignment apertures, have their intensity reduced (≈0.5 mW to avoid saturating the absorption), and are carefully overlapped with a beam splitter and a pair of periscopes. We find that careful overlap is essential for precise ratios and system linearity. If the two probe lasers sample different spaces, they are more sensitive to shot-to-shot variations in the evolution of the ablation plume. The overlapped beams are focused (500 mm focal length lens) to a diameter of ≈0.1 mm and have height above the sample surface (typically 2–3 mm) adjusted to give maximum absorption signal. After passing out of the ablation chamber the two probe beams are separated on a 3600 l/mm holographic grating and detected with amplified Si photodiodes (Thorlabs PDA36A).

Transient signals from the photodiodes are digitized with a National Instruments PXI-6120 data acquisition card that has four independent high speed (800 kHz) 16-bit analog-to-digital converters (ADCs). The ADCs are externally triggered by a pulse generation network that samples the photodiodes just before firing the ablation laser, and again after firing with an adjustable delay set to the absorption maximum. These interleaved measurements correspond to incident and transmitted laser intensities, I_o and I_t, for a conventional absorption determination and are stored in a single waveform (for each line of the sample raster scan) as a sequence of (I_o, I_t)-pairs. This acquisition mode was needed to support the high-repetition-rate ablation laser and, in principle, could support measurement rates up to half the maximum sampling rate of the ADCs. Measuring time-resolved I_o and I_t on a single detector for each isotope was also found to have better baseline noise (minimum detectable single-shot absorbance $<\approx 10^{-3}$) than having beam splitters and separate I_o detectors before the ablation chamber, and is mechanically less complex. Baseline offsets for the detectors were determined at the beginning of each sample raster scan line using a computer controlled shutter to block the probe lasers, and was important for accurate determination of strong absorption. The overall system is controlled by a LabView (National Instruments) program that reads, processes, and stores the data from the ADCs during synchronized raster scanning of the sample. The LabView program also reads data from the WA1500 wavemeter (every 2 s) using control shutters that switch between probe lasers, and provides feedback voltages to tune and/or stabilize laser frequency drift via piezoelectric transducer control of the laser cavity gratings.

2.2. Samples

Initial spectroscopic studies of the isotopic structure used metallic gadolinium foil of 0.25 mm thickness and nominally natural isotopic abundance (Alfa-Aesar, 99.9% purity). Small pieces (≈0.5×1 cm) were mounted on the sample carrying stage with double-sided photo mounting tape and used without further treatment. The metallic targets were used primarily for system development and spectroscopic studies [18].

Particulate samples of $GdCl_3 \cdot xH_20$ with varying isotopic composition were prepared from two samples of Gd_2O_3, highly enriched in ^{152}Gd (5 mg, 30.6%) or ^{160}Gd (10 mg, 98.2%), obtained from Medical Isotopes, Inc. Portions of these were dissolved in small volumes (typically 0.3 ml) of 7% HCl to make stock solutions of known concentration. Portions of these were then volumetrically mixed to produce new solutions with desired isotope ratio $R(^{152}Gd{:}^{160}Gd)$. Small volumes were pipetted onto microscope slides and dried at 120 °C for several hours. The resulting solid residue was removed from the slide with a razor blade and could be used directly for 'bulk' studies, or finely ground for 'particulate' studies. Grinding was done between two sheets of 400 grit 'wet or dry' carborundum sandpaper. Microscopic examination of the fine-ground material (see Fig. 2) showed particles ranging in size from sub-micron to ≈20 μm diameter, with most between 1 and 5 μm. Both 'bulk' and particulate samples were mounted for measurement by spreading on a microscope slide with a camel-hair brush and, for the smaller particulates, tapping the slide upside-down to dislodge larger clumps. Double-sided photo mounting tape was used to pick up the dispersed materials from the microscope slide and mounted on the sample carrier stage. Typical $R(^{152}Gd{:}^{160}Gd) = 0.01$, 0.04 and 0.30 served as simulants for ^{235}U:^{238}U with near natural, low enriched (LEU, as used by commercial power reactors), and highly-enriched uranium (HEU). For some measurements, the fine-ground particulates were mixed in

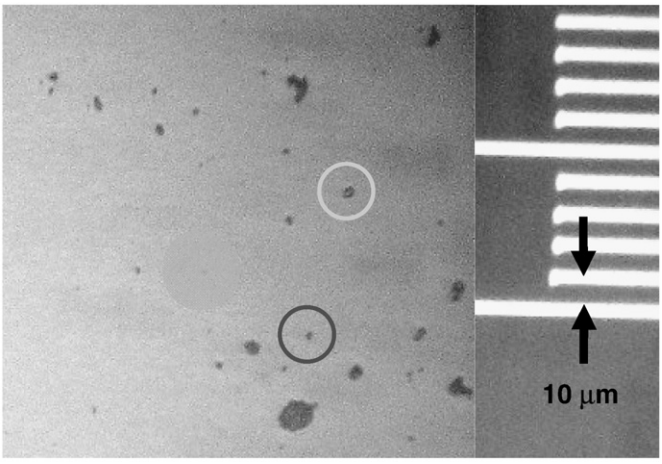

Fig. 2. Microscopic image of $GdCl_3 \cdot xH_20$ particulate sample. The ablation laser spot size is ≈20 μm, while the light circle highlights a particle (≈2 μm) at the lower end of the range where low enrichment (1%) can be measured, and the dark circle shows the size limit (≈1 μm) for determination of isotope ratio for a highly-enriched (30%) particle.

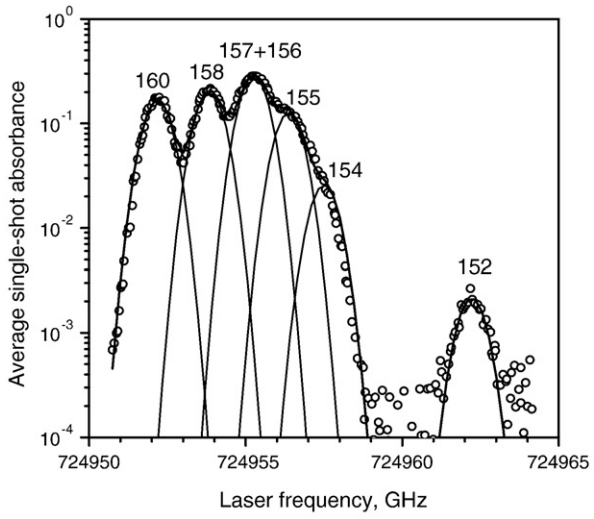

Fig. 4. Isotopic structure in the Gd $4f^7 5d6s^2\ ^9D_4^o \rightarrow 4f^7 5d6s6p\ ^9D_3$ transition at 413.4 nm.

with excesses of 'dust' to simulate what might be expected in collected environmental samples. For this purpose, we used finely powered Columbia River sediment (NIST standard reference material 4350B); the $GdCl_3 \cdot xH_20$ particles were added to a weighed amount of sediment powder and thoroughly mixed with a micro spatula and vigorously shaken in a capped weighing bottle.

3. Results and discussion

3.1. Spectroscopic studies

Fig. 3 gives a partial energy level diagram for neutral atomic gadolinium showing the two transitions used in these experiments. Other transitions in the same region were studied by diode laser induced fluorescence spectroscopy [19], but did not measure isotope shifts for the transitions shown in Fig. 3. Thus, high-resolution isotopic spectra of each transition were obtained using a sample of metallic Gd foil with natural isotopic abundances. The frequency of a given probe laser was scanned slowly over the transition of interest while the sample was continually rastered to provide fresh material to the ablation laser. Fig. 4 shows the spectrum observed for the 413.4 nm transition. The signal was averaged for 10 ablation shots at each point, and to account for laser scan nonlinearity, the probe-laser frequency was read by the wavemeter at each point. The observed peaks were fit with Gaussian profiles with equal widths. Formally, the different isotopes should have different Doppler widths inversely proportional to the square-root of the masses, but this is only a 2.5% difference between ^{160}Gd and ^{152}Gd, and allowing free widths for all peaks often gave erroneous results for the poorly resolved ^{155}Gd and ^{154}Gd components. The resulting Gaussian fit width (FWHM) of 0.806(20) GHz corresponds to normal Doppler broadening at a temperature of 376(19) K (for ^{156}Gd), indicating that the ablated material has almost completely thermalized with the surrounding cover gas by the time of the absorption measurement, ≈150 μs after the ablation pulse. Comparison with Doppler-free atomic beam spectroscopy on a similar transition, $6s^2\ ^9D_6^o \rightarrow 6s6p\ ^9F_7$ at 422.7 nm [20], indicates that the hyperfine structure for the odd isotopes ^{155}Gd and ^{157}Gd is probably smaller than the Doppler width observed in the current work, and that the peak labeled 156 + 157 in Fig. 4 is likely an unresolved blend of ^{156}Gd and ^{157}Gd. This is supported by areas under the fit peaks that closely reproduce the isotopic abundances: the fit 156 + 157 peak contain 35.4% of the total area, while the combined abundance of ^{156}Gd (20.5%) and ^{157}Gd (15.7%) is 36.2%. The isotope shift observed between ^{152}Gd and ^{154}Gd is more than three times larger than between ^{158}Gd and ^{160}Gd, which is attributed to nuclear symmetry breaking between neutron numbers 88 and 90 and the transition from a spherical to deformed nucleus [20].

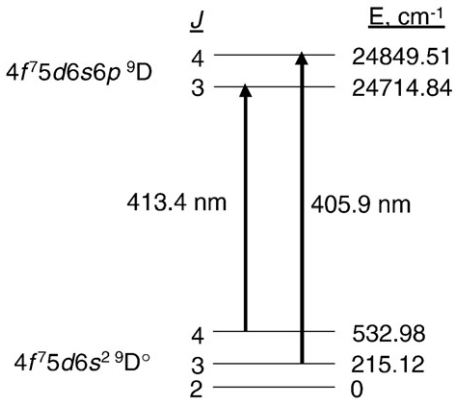

Fig. 3. Energy levels and transitions used for dual wavelength measurement of gadolinium isotope ratios.

The $J = 3 \rightarrow 4$ transition at 405.9 nm exhibited isotopic structure quite similar to that shown in Fig. 4 and is not presented here. The absolute transition frequencies (GHz) for the fit isotopic peaks for the two transitions are given in Table 1. Since the ^{154}Gd peak appears only as a shoulder and may be blended with some of the ^{155}Gd hyperfine structure, the values reported for ^{154}Gd may have additional uncertainty (estimated at 0.2 GHz) beyond that given in the table.

Table 1
Measured transition frequencies for isotopes of gadolinium.

Isotope (% nat)	Absolute transition frequencies, GHz	
	$J = 4 \rightarrow 3$, 413.41 nm	$J = 3 \rightarrow 4$, 405.94 nm
152 (0.2)	725,962.25(13)	738,528.53(7)
154 (2.2)	724,957.04(17)	738,523.47(6)
155 (14.7)	724,956.23(14)	738,522.51(7)
156 + 157 (20.5 + 15.7)	724,955.25(9)	738,521.57(5)
158 (24.9)	724,953.84(7)	738,520.23(4)
160 (21.9)	724,952.20(6)	738,518.58(4)

Uncertainties are the standard deviation for 3–5 repeated measurements with 0.03 GHz instrumental uncertainty added for the WA1500 wavemeter.

3.2. Isotope ratio measurements

3.2.1. Normalization of transition strengths

Isotope ratio measurements are made on a shot-by-shot basis simply by holding the two probe lasers on frequency for the targeted isotopes, as given in Table 1. Since two different atomic transitions are used to monitor the targeted isotopes, ratios must be normalized for the relative oscillator strength of the two transitions. This was done by tuning both probe lasers for ^{160}Gd in their respective transitions and comparing the absorbance in the two channels. The 405.94-nm $J=3\rightarrow4$ transition was found to be 4.5(3) times stronger than the $J=4\rightarrow3$, 413.41-nm transition. Although both lasers are probing ^{160}Gd, there is no 'crosstalk' from saturation effects because the transitions use different lower and upper levels. Also, both transitions begin in low-lying metastable levels of different energies and are thus expected to have different thermal populations. Correction for the thermal populations is implicitly contained in the experimental measurement of ^{160}Gd:^{160}Gd absorption ratios, but might be expected to change with widely varying ablation conditions or measurement delay time. Any given measurement of the effective ratio is considerably more precise ($\approx$1%); the $\approx$7% uncertainty quoted above represents day-to-day variations that may include thermal population effects as well as variations from imperfect collinear alignment of probe beams, and hence systematic error from sampling different parts of the ablation plume. In ratio measurements, the stronger 405.94-nm transition is used to monitor the minor ^{152}Gd isotope to effectively increase the dynamic range. Best precision is obtained if the ^{160}Gd:^{160}Gd calibration is performed routinely; generally this is done at the beginning of each day, but also whenever there is a realignment of the probe beams.

3.2.2. Signal level discrimination

A sensible isotope ratio measurement requires sufficient signal for both isotopes, particularly for ^{160}Gd, the ratio denominator. However, using only the ^{160}Gd absorption signal as a discriminator for valid measurement leads to systematic bias that rejects particles highly enriched in ^{152}Gd (and hence less ^{160}Gd). Thus we define combined weighted absorbance as:

$$A_C = A(^{160}Gd) + A(^{152}Gd) / 4.5,$$

where the factor of 4.5 corrects for greater oscillator strength in the ^{152}Gd transition. This formulation gives a constant A_C value for equal amounts of Gd, regardless of the (assumed binary) isotopic composition. The minimum detectable single-shot absorbance was determined from the distribution of single-shot absorbance for a blank sample mounting tape and one heavily loaded with SRM 4350B powder (without added Gd-bearing particles). Results are shown in Fig. 5. In both cases the width of the 'zero-point' absorption distributions is $\approx 6\times10^{-4}$ A (FWHM $=2\sigma$). The blank mounting tape has a negligible offset, but the loaded SRM blank does have an offset of $\approx 3\times10^{-4}$ A, which does not seem to be greatly wavelength dependent and may be due to scattering and refraction effects with the greater quantity of material ablated. The noise width of the zero-point absorption ultimately limits measurement sensitivity. Typically, the A_C discriminator value is set at 5–10 times the zero-point width to have sufficient signal for valid ratio measurement. If the zero-point offset is significant (e.g., emission or bulk absorption) this can be analyzed and corrected during data post-processing.

3.2.3. Mixed 'bulk' samples of $GdCl_3 \cdot xH_20$ with different isotopic ratios

Fig. 6 shows the results for a sample of mixed 'bulk' $GdCl_3 \cdot xH_20$ particles where typical particle diameters range from $\approx$30 to 300 μm. Prepared as described in Section 2.2, the sample is a ternary mixture of particles with $R(^{152}Gd:^{160}Gd) = 0.0094$, 0.047, and 0.43. By weight, there are nearly equal amounts of the $R=0.0094$ and $R=0.047$ components,

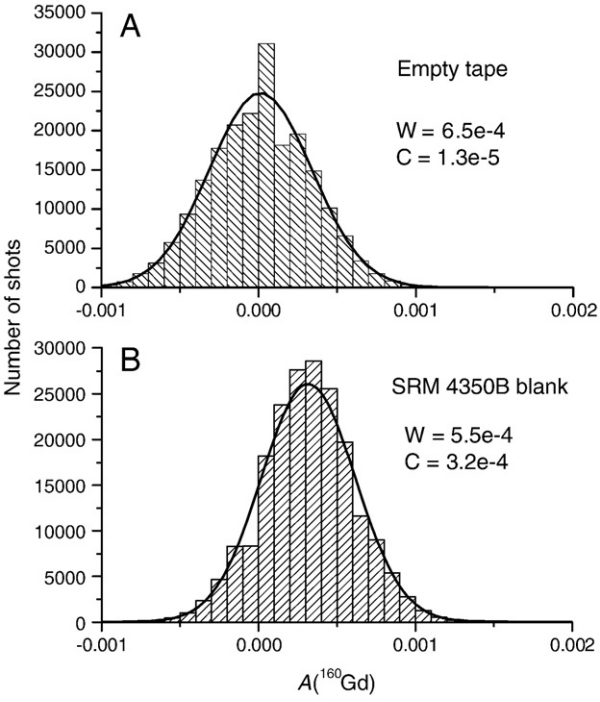

Fig. 5. Distribution of single-shot absorption for blank sample mounting tape and for a 'heavy' load of SRM 4350B dust. W and C are width (FWHM) and center of the peak in absorbance units.

and $\approx$5% with highly enriched $R=0.43$. Fig. 6(A) shows the spatial map of the measured ratios: scanning resolution is 0.02×0.03 mm in the x- and y-dimensions, respectively (500×400 pixels for a total of 200,000 laser shots collected in 17 min). Areas in white had combined absorbance, $A_C<0.05$. Fig. 6(B) shows the measured ratios as a function of A_C for all ablation shots. The vertical red line marked 'DISC' is $A_C=0.05$; points to the left of this line are shown as white in Fig. 6(A) and are excluded from subsequent statistical analysis. The three different components can be seen in the plot and there appears to be no bias in the ratios as a function of signal level or particle size. Fig. 6(C) shows a histogram of the isotope ratios for those ablation shots with $A_C\geq0.05$; out of 200,000 ablation laser shots, 10,540 exceeded this discrimination threshold. Each of the peaks in the histogram is fit with a Gaussian profile, from which the center is used to calculate measured R and the area is used to evaluate preponderance of the particle type. These are shown in Fig. 6(C) with the values in parentheses as (^{152}Gd:^{160}Gd ratio, % of total discriminated shots); the R-values expected from the gravimetric/volumetric sample preparation are shown in red for reference. Generally, the determined isotope ratios are in good agreement with the expected values. The $R=0.0115$ peak is about 20% too high, but is still within the estimated uncertainty of the sample preparation. The relative areas under the peaks are also qualitatively in agreement with the preparation expectations although the $R=0.412$ peak area is a bit low. This is attributed to difficulties in getting quantitative transfer of the particles from the preparation microscope slide to the sample mounting tape. The summed area for the three fit peaks is only 89.1% of the total shots with $A_C\geq0.05$ and is attributed to two factors: (1) the lowest ratio peak has very weak ^{152}Gd absorbance and systematic electronic noise contributes broad tails that are not well described by the Gaussian distribution. (2) There is filling of the valleys between the peaks due to shots which simultaneously sample more than one of the particle types, for example, along the border between the 'red' and 'green' particles at the lower left in Fig. 6(A). These 'combined particle' shots are seen in Fig. 6(B), most clearly between the $R=0.0115$ and $R=0.0492$ peaks; some of these shots have quite strong signals but clearly lie outside the single particle type distributions. The combined particle nature of these shots is further

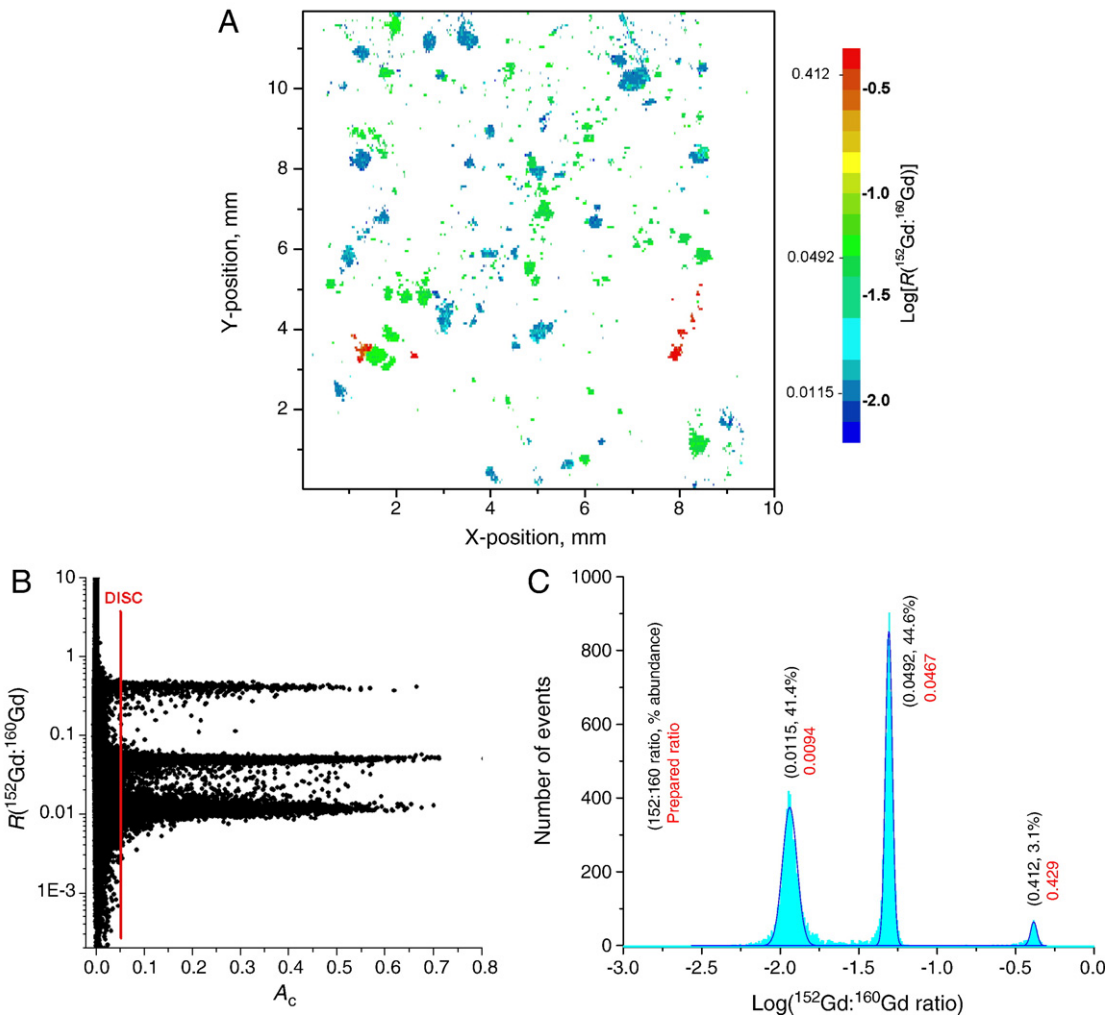

Fig. 6. Isotope ratio measurements on $GdCl_3 \cdot xH_2O$ 'bulk' sample containing three components with different ^{152}Gd:^{160}Gd ratios. (A) Spatial map of ratios. (B) Shot-by-shot ratios as a function of A_C for all shots. (C) Histogram of discriminated ($A_C > 0.05$) isotope ratios, shown on a logarithmic scale so that the low isotope ratio peaks can be seen clearly.

confirmed by the fact that they are observed only between peaks but not above the high-R peak, nor below the low-R peak, as might be expected for a systematic noise process. This 'valley filling' becomes more pronounced with more finely dispersed, highly mixed or heavily loaded samples (see Fig. 7 and discussion below). In Fig. 6(B), it can been seen that the discriminator level setting of $A_C \geq 0.05$ is fairly conservative; if reduced to 0.01, the major effect is to broaden the tails of the low-R peak in Fig. 6(C), with little effect on the two higher peaks.

3.2.4. Isotope ratios in finely dispersed micron-sized particles

As described in Section 2.2, micron-sized particles were prepared by grinding the bulk $GdCl_3 \cdot xH_20$ between sheets of 400 grit sandpaper. These fine-ground powers were further mixed with powdered 'dirt' (NIST SRM 4350B, Columbia River sediment) to simulate environmental samples. One disadvantage of this approach is that it is difficult to get quantitative transfer of the ground powders from the sandpaper and quantities were too small to be accurately measured with the available laboratory balance (0.1 mg resolution); thus, type compositions are only approximate. Fig. 7 shows results for samples of this type, where ground $GdCl_3 \cdot xH_20$ particles were mixed with an ≈20-fold excess of SRM 4350B. Fig. 7(A) shows the spatial map for a sample containing a binary mixture with approximately equal amounts of $R = 0.01$ and $R = 0.032$ particles. In Fig. 7 color coding is restricted to a scheme that might be used for screening uranium bearing particles, with four ranges corresponding to near natural abundance or below ($R < 0.015$, blue), low enrichment ($R = 0.015$–0.08, cyan), low enrichment but greater than expected for normal power reactor production ($R = 0.08$–0.2, green), and highly enriched ($R > 0.20$, red). The outline of the sample mounting tape can be clearly seen and, although there are a few larger clumps, the Gd-bearing particles appear to be well dispersed. Fig. 7(B) zooms in on a 1 mm^2 area (50 × 50 ablation shots) of the data shown in (A) to more clearly show the particle and ratio distributions. Fig. 7(C) shows a 1 mm^2 zoom on a similarly prepared sample with an ≈1:3 mix of the $R = 0.01$ and $R = 0.032$ particles and spiked with ≈5% highly-enriched (HE, $R = 0.43$ ratio) particles. Again, the fine dispersion of the particles can be seen and the sparse HE particles are readily apparent. Figs. 7(D) and (E) show the measured ratio distributions for the binary mixture (shown in maps A and B) and the HE spiked sample (map C), respectively. The peak resolution for these micron-sized particles is not as good as for the 'bulk' material (see Fig.6(C)), largely because of the lower signal levels, but also because there is greater filling of the valleys between the peaks because, with the finely dispersed small particles, it is more likely that multiple particles will be present within the ablation laser spot size. Nonetheless, the signature from the relatively low number of highly-enriched particles (red area in Fig. 7(E)) is readily apparent.

To test the capability for detection of highly-enriched particles near the limit of detection, a sample similar to those shown in Fig. 7 was prepared with equal amounts of $R = 0.01$ and $R = 0.032$ particles, but the total Gd particle:SRM 4350B weight fraction was reduced from 5% to 0.08%, and the fraction of HE particles were reduced from 5% to 0.5%. Also, the sample scan area was increased to 20 × 20 mm with

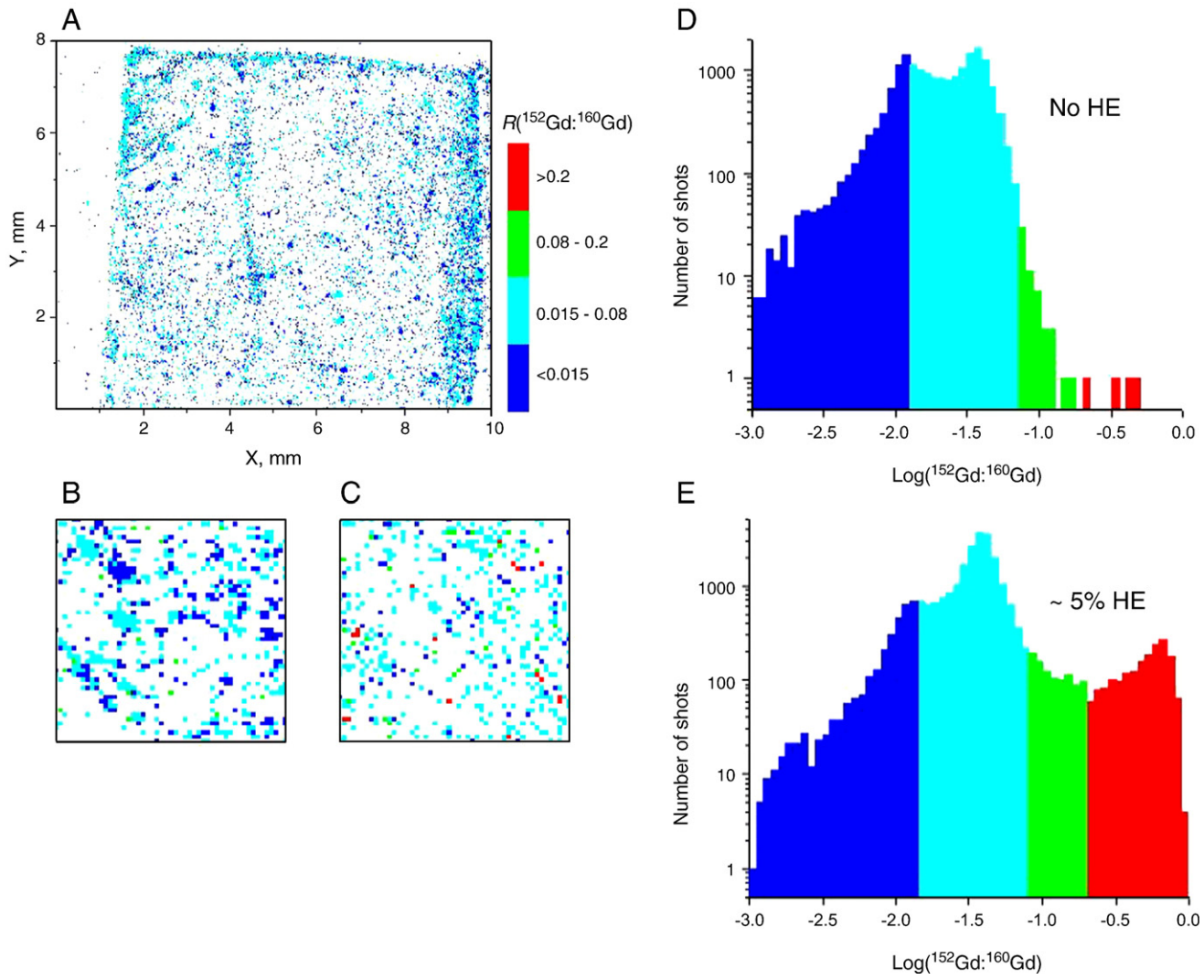

Fig. 7. (A) Image of raster scanned sample tape, color coded for ^{152}Gd:^{160}Gd ratio, white indicates no signal sufficient for ratio determination (A_C<0.006). (B) Zoom to 1 mm^2 area of (A). (C) Zoom on similar sample but containing ≈5% of highly enriched (R>20%) ^{152}Gd. (D) and (E) are distributions of isotope ratios for the two samples. In the 'No HE' sample there are equal amounts of R = 0.01 and R = 0.032, while in the '5% HE' sample there is roughly a 1:3 mix of R = 0.01 and R = 0.032 particles.

0.020×0.025 mm resolution for a total of 800,000 shots (≈70 min). Fig. 8(A) shows a plot of measured ratio vs. A_C for all shots on a blank sample of the SRM (without added Gd-bearing particles), while Fig. 8 (B) shows similar results for the sample. Fig. 8(C) shows a ratio histogram for those shots exceeding a discriminator level of A_C> 0.008. In the histogram the two major component peaks are fit with

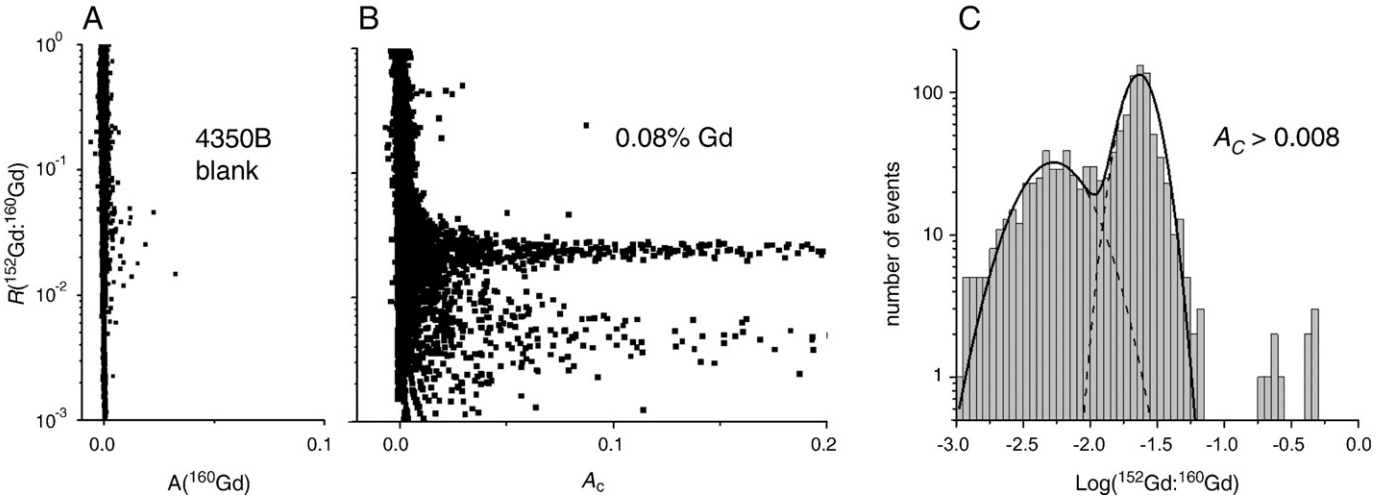

Fig. 8. Trace detection performance for high-enrichment particles. (A) Signal from a blank sample of SRM 4350B. (B) SRM 4350B spiked with 0.08% Gd-bearing particles: shot-by-shot isotope ratios as a function of combined weighted absorbance. (C) Isotope ratio distribution for valid absorbance data, A_C>0.008.

Gaussian profiles and, although the heights and widths are different because of the increased relative noise level for ^{152}Gd in the low ratio particles, the areas of the two peaks are nearly equal. Out of the 800,000 lasers shots there were 1178 Gd-bearing particles detected, and of these 10 were highly enriched with measured $R>0.2$. These few events can be seen in both plots 8(B,C) and the HE particle fraction of 0.8(3)% is consistent with expectations from the sample preparation. Finally, for the blank shown in Fig. 8(A), there were only 17 valid events with $A_C>0.006$. Most of these have $R=0.01$–0.05 and may be cross contamination from prior sample preparations and/or measurements. However, there was only one valid HE positive event with $R>0.2$.

4. Conclusions

We have used prepared samples of gadolinium-bearing particles with different isotopic distributions as surrogates to demonstrate the feasibility of Laser Ablation-Absorption Ratio Spectrometry (LAARS) as an approach to isotope ratio analysis for characterization of environmental aerosol samples containing traces of enriched uranium. It has been show that, by using two diode lasers to simultaneously monitor two different isotopes in different atomic transitions, isotope ratios can be accurately and reproducibly measured on a shot-by-shot basis and that sensitivity is sufficient to measure low ratios, to less than 1% for individual micron-sized particles. This corresponds to single-shot detection limits approaching the femtogram range. The method appears to be quite immune to background from other particles or materials that do not contain compounds of the element targeted for ratio measurement. Highly-enriched particles have very distinctive signatures and can be unambiguously identified, even when they are present for only a few out of $\approx 10^6$ sampling laser shots. A method using triggered asynchronous ADC sampling has been presented for obtaining high-precision shot-by-shot transmittance data at high ablation laser rates, which allows significantly greater sample throughput and/or spatial resolution (for a given measurement time). Measurement performance is largely independent of chemical composition and does not require sample preparation since laser ablation atomizes the sample (although bulk metallic samples give signals 3–5 times greater signal than bulk salts). Work is now underway to evaluate LAARS for isotope ratio analysis on micron-sized uranium bearing particles and to integrate with an automated aerosol collection system.

Acknowledgement

This work was performed under a PNNL Laboratory Directed Research and Development Program. Pacific Northwest National Laboratory is operated for the U.S. Department of Energy by Battelle Memorial Institute under Contract No. DE-AC05-76RL01830.

References

[1] J.C. Miller, R.F. Haglund, Laser Ablation and Desorption, 1st ed, Academic Press, San Diego, 1998.
[2] R.E. Russo, X. Mao, H. Liu, J. Gonzalez, S.S. Mao, Laser ablation in analytical chemistry — a review, Talanta 47 (2002) 425–451.
[3] D.A. Cremers, L.J. Radziemski, Handbook of Laser-Induced Breakdown Spectroscopy, John Wiley & Sons, Chichester, 2006.
[4] B.W. Smith, A. Quentmeier, M. Bolshov, K. Niemax, Measurement of uranium isotope ratios in solid samples using laser ablation and diode laser-excited atomic fluorescence spectrometry, Spectrochim. Acta Part B 54 (1999) 943–958.
[5] A. Quentmeier, K. Niemax, M. Bolshov, Measurement of uranium isotope ratios in solid samples using laser ablation and diode laser-atomic absorption spectrometry, Spectrochim. Acta Part B 56 (2001) 45–55.
[6] H. Liu, A. Quentmeier, K. Niemax, Diode laser absorption measurement of uranium isotope ratios in solid samples using laser ablation, Spectrochim. Acta Part B 57 (2002) 1611–1623.
[7] P.A. Voigt, Measurement of U I and U II relative oscillator strengths, Phys. Rev. A 11 (1975) 1845–1853.
[8] R. Avril, A. Ginibre, A. Petit, On the hyperfine structure in the configuration $5f^3 6d7s^2$ of neutral uranium, Z. Phys. D 29 (1994) 91–102.
[9] R. Avril, M.D. Labachellerie, F. Viala, A. Petit, The hyperfine structure of 2 and 4 eV levels in uranium, J. Less-Common Met. 122 (1986) 47–53.
[10] H.-D.V. Böhm, W. Michaelis, C. Weitkamp, Hyperfine structure and isotope shift measurements on ^{235}U and laser separation of uranium isotopes by two-step photoionization, Opt. Commun. 26 (1978) 177–182.
[11] W.J. Childs, O. Poulsen, L.S. Goodman, High-precision measurement of ^{235}U ground-state hyperfine structure by laser-rf double resonance, Opt. Lett. 4 (1979) 35–37.
[12] W.J. Childs, O. Poulsen, L.S. Goodman, High-precision measurement of the hyperfine structure of the 620-cm^{-1} metastable atomic level of ^{235}U by laser-rf double resonance, Opt. Lett. 4 (1979) 63–65.
[13] S. Gerstenkorn, P. Luc, C. Bauche-Arnoult, D. Merle, Structure hyperfine du niveau fondamental, moments dipolaire et quadrupolaire de l'isotope 235 de l'uranium, J. Phys. (Paris) 34 (1973) 805–812.
[14] L.A. Hackel, C.F. Bender, M.A. Johnson, M.C. Rushford, Hyperfine structure measurement of high-lying levels in uranium, JOSA 69 (1979) 230–232.
[15] D.J.H. Wort, C.G. Brown, R.D. Plumbe, The hyperfine structure of the 4 eV odd-levels in uranium, J. Phys. E Sci. Instrum. 12 (1979) 829–832.
[16] J. Blaise, L.J. Radziemski Jr., Energy levels of neutral atomic uranium (U I), J. Opt. Soc. Am. 66 (1976) 644–659.
[17] R.J. Engleman, B.A. Palmer, Precision isotope shifts for the heavy elements. I. Neutral uranium in the visible and near infrared, JOSA 70 (1980) 308–317.
[18] N.C. Anheier Jr., M.D. Wojcik, B.D. Cannon, B.A. Bushaw, Uranium Isotopic Assay Instrument. Addressing Verification Challenges, Proceedings of an International Safeguards Symposium, Oct 16-20, 2006, paper IAEA-CN-148/33, IAEA, Vienna, Austria, 2006.
[19] H. Niki, T. Tanikawa, S. Tokita, Y. Izawa, Measurement of hyperfine structure and isotope shift of transitions in gadolinium using blue diode laser, Jpn. J. Appl. Phys. 44 (2005) 6075–6078.
[20] K. Blaum, B.A. Bushaw, S. Diel, C. Geppert, A. Kuschnick, P. Müller, W. Nörtershäuser, A. Schmitt, K. Wendt, Isotope shifts and hyperfine structure in the [Xe] $4f^7 5d6s^2\ ^9D_J$–[Xe] $4f^7 5d6s6p\ ^9F_{J+1}$ transitions of gadolinium, Eur. Phys. J. D 11 (2000) 37–44.